The Astrophysical Journal Supplement Series, 143:455–467, 2002 December

SINGLE-PHOTON INFRARED EMISSION SPECTROSCOPY OF GASEOUS POLYCYCLIC AROMATIC HYDROCARBON CATIONS: A DIRECT TEST FOR PROPOSED CARRIERS OF THE UNIDENTIFIED INFRARED EMISSION BANDS

Hack-Sung Kim[1] and Richard J. Saykally
Department of Chemistry, University of California, Berkeley, CA 94720-1460; saykally@uclink.berkeley.edu
Received 2002 May 28; accepted 2002 July 22

ABSTRACT

We describe the measurement of infrared emission from excited gas-phase polycyclic aromatic hydrocarbons (PAHs) cations by an electron-impact ion beam reflectron system coupled to our "single-photon infrared emission" (SPIRE) spectrometer. This experiment provides for direct comparison of laboratory infrared emission spectra of gaseous ionized PAHs with the "unidentified infrared emission bands" (UIRs), the origin of which is still debated. We present results for the pyrene cation ($C_{16}H_{10}^+$) and the dehydrogenated pyrene cations ($C_{16}H_8^+$ and $C_{16}H_6^+$) showing general agreement between the corresponding SPIRE bands and UIR features, although it is not a detailed match. We also discuss possible contributions from the pyrene dimer cation $(C_{16}H_{10})_2^+$.

Subject headings: dust: extinction — infrared: ISM — ISM: lines and bands — methods: laboratory — molecular data — techniques: spectroscopic

1. INTRODUCTION

Definitive identification of the carriers responsible for the "unidentified infrared emission bands" (UIRs) continues to be a central activity in molecular astrophysics since these are believed to constitute a significant reservoir of carbon and may be precursors of biogenic molecules (Bernstein et al. 1999). Current models favor a mixture of neutral and cationic polycyclic aromatic hydrocarbons (PAHs; Allamandola, Tielens, & Barker 1985; Léger & Puget 1984), perhaps supplemented by the presence of hydrogenated amorphous carbon (Kwok, Volk, & Bernath 2001). Efforts to reproduce the UIR features in the laboratory have established the general connection with PAHs (Allamandola, Hudgins, & Sandford 1999), but up to this point, no specific molecule has been identified as a probable carrier.

Our group has developed an infrared photon-counting experiment based on a Blocked Impurity Band Solid State Photomultiplier (BIB-SSPM; Petroff, Stapelbroek, & Kleinhans 1987) to measure gas-phase IR emission from UV laser-excited neutral PAHs over the entire spectral region spanned by the UIRs. We call this technique single-photon infrared emission spectroscopy (SPIRES; Cook et al. 1996, 1998) since a single incident IR photon is capable of generating a measurable voltage pulse. With this experiment, we have examined IR emission spectra of a large collection of neutral PAHs, finding that none of them are likely to be a major contributor to the UIRs (Cook et al. 1996, 1998; Schlemmer et al. 1994; Wagner 2001; Wagner, Kim, & Saykally 2000).

The detection of mid-IR emission from gas-phase ions is a formidable technical challenge. Typical ion currents ($\sim$2 μA at the field of view of the monochromator in the SPIRE spectrometer) correspond to number densities of only 10^6–10^7 cm^{-3}, and even lower densities are obtained in ion traps. Moreover, the average lifetime of gas-phase ions (without an ion trap) is usually short ($\sim 10^{-5}$ s in our system). To effectively use the BIB-SSPM, the detector must be cooled below $\sim$7 K and shielded from blackbody radiation emitted by the surroundings. Since the detector is saturated at count rates near 10^8 photons (s cm^2)$^{-1}$, the entire spectrometer must be maintained at temperatures lower than $\sim$15 K, and all optical elements in the field of view of the detector must generate a negligible blackbody photon flux over the entire spectral region of interest. Hence, ion optics in the field of view of the detector must be cooled to $\sim$77 K, and the diameter of the ion beam aperture in the field of view of the detector must be minimized. Since the space charge–limited ion current is inversely proportional to the square root of molecular mass, the maximum achievable ion current of molecules with high molecular mass (e.g., PAHs) is lower than that of molecules with low mass, for constant aperture. Therefore, it is difficult to achieve a current density of excited PAH ions at the final aperture in the field of view of the detector that is high enough to yield detectable mid-IR emission in the cryogenic environment.

Nevertheless, we recently reported the first observation of gas-phase IR emission spectra from excited PAH cations (Kim, Wagner, & Saykally 2001). The measured SPIRE spectrum of the pyrene cation ($C_{16}H_{10}^+$) agrees well with the general appearance of UIR features, thus providing support for the role of the cations in the "PAH hypothesis" (Allamandola, Tielens, & Barker 1985; Léger & Puget 1984). Here we present a detailed analysis of the data, evidencing emission spectra from the dehydrogenated pyrene cations ($C_{16}H_8^+$ and $C_{16}H_6^+$) as well as the pyrene cation. Our SPIRES experiment can provide a direct test for the possible contribution of a given PAH$^+$ to the UIRs. Also, Oomens et al. (2000, 2001) have developed an impressive *absorption* experiment based on photodestruction of trapped ions, wherein the internal energy-dependent redshifts in vibrational transitions are measured by controlling the trapping time. These two experiments are thus capable of contributing definitive new insights into the origin of the UIRs.

[1] Present address: Institute for Environmental Catalysis, Northwestern University, Evanston, IL 60208; hskim@northwestern.edu.

2. EXPERIMENTAL

PAH ions were generated by electron-impact ionization of thermally generated PAH vapor. It is well known that a single molecular ion peak dominates the mass spectrum of ionized PAH generated by electron-impact ionization, as a consequence of the high activation energies required for fragmentation. The primary ionic species produced for pericondensed PAHs like pyrene (Wacks 1964) are thus the parent monocation ($C_{16}H_{10}^+$), followed by the dehydrogenated cations ($C_{16}H_9^+$, $C_{16}H_8^+$, etc.), and the dications ($C_{16}H_{10}^{2+}$, $C_{16}H_8^{2+}$).

The expected physical state of interstellar PAHs emitting the UIRs excited by the absorption of UV (or far-UV) photons (Tielens 1997) corresponds to vibrationally hot (~900 K; Joblin et al. 1994) and rotationally cold (~100 K; Rouan et al. 1992) molecules. Unanswered questions at the outset of the PAH ion beam experiments were whether the molecules would become sufficiently vibrationally excited by the electron-impact event and whether the electron-impact excitation would resemble the absorption of UV photons. We show that this is indeed the case.

Classically, electron impact behaves like a short-pulse light source, in view of a time-dependent electric field interacting with the molecule (Brion & Hamnett 1981). The typical effective pulse duration is subfemtosecond, and it is well established that electron-impact excitation mimics photoabsorption (optical dipole excitation) at high impact energies (Keller, Coplan, & Goruganthu 1992). High vibrational excitation was observed in benzene (Wong & Schulz 1975) and coronene (Khakoo, Ratliff, & Trajmar 1990), and it is a general characteristic of electron-impact ionization. Maier & Marthaler (1978) observed IR emission spectra from electron-impact ionized *p*-dichlorobenzene cations. The electronically excited PAH (ion) relaxes by rapid internal conversion to the ground electronic state, and the electronic energy is then distributed among the various vibrational modes (internal vibrational redistribution [IVR]). The vibrational temperature of the *ground* electronic state of the PAH ion (on which IR emission will occur) after IVR, produced by electron impact in effusive beam, can also be determined empirically. IVR has been observed in electron-impact excited emission spectrum of *p*-difluorobenzene (Furuya, Koto, & Ogawa 1996) as well as in laser experiments (Engelhardt et al. 2001). Therefore, we can conclude that electron-impact excitation mimics photoabsorption reasonably closely in the present context and also should approximate the UIR mechanism (Allamandola, Tielens, & Barker 1989; Léger & d'Hendecourt 1989), except for the low rotational temperature (Rouan et al. 1992). In our experiments, the rotational temperature is estimated to be near the oven temperature (ca. 340 K). We will discuss it later.

We used the same equipment as for the PAH desorption experiments (Cook et al. 1996, 1998; Schlemmer et al. 1994; Wagner 2001; Wagner et al. 2000). The design and performance of an electron-impact ion beam reflectron system coupled to our SPIRE spectrometer were briefly described in a recent paper (Kim et al. 2001) and will be described in detail in another paper (Kim & Saykally 2002). We will discuss the detailed analysis of the SPIRE spectra in the following section.

3. RESULTS AND DISCUSSION

The SPIRE spectrum in Figure 1 (trace *b*) was obtained in the 5.5–8.5 μm region when the ions generated by the electron impact of pyrene vapor were injected into the reflectron region (Kim et al. 2001). The SPIRE background spectrum in Figure 1 (trace *c*) was obtained when the ions were deflected before entering the monochromator field of view under the same conditions.

IR emission in Figure 1 (trace *b*) is attributed to cationic species generated by electron impact of pyrene vapor for the following reasons: First, the ion optics and quadrupole electric field retard any *anions* moving toward the reflectron region, according to SIMION ion beam simulation (Dahl 1995). Therefore, anionic species cannot contribute to our spectra. Second, the ion current was measured at the last ring of the stack closest to the monochromator when the cations were injected into the reflectron region. Therefore, gas-phase cations definitely exist at the monochromator field of view during the signal scan. Third, the background spectrum in Figure 1 (trace *c*), which was obtained when the ion current was almost zero in the monochromator field of view, is essentially flat over the entire spectral range studied. If excited *neutral* species induced by electron impact had emitted IR radiation in the spectral range studied, the background spectrum would have shown some spectral features due to those species. Fourth, the IR spectrum of the pyrene cation shows very different features from those of neutral pyrene, and the major features observed in the our emission spectrum in Figure 1 (trace *b*), except for extra bands in the 5.8–6.1 μm (1639–1724 cm^{-1}) and 7.7–7.8 μm (1282–1299 cm^{-1}) ranges, agree well with the calculated IR spectrum, cryogenic matrix IR absorption spectra, and gas-phase IR absorption spectrum of the pyrene cation ($C_{16}H_{10}^+$), as shown in Figures 1 and 2 and in Table 1. Finally, according to mass spectral intensities (Wacks 1964), the molar ratios of cations generated by a 70 V electron impact of pyrene at 80°C (2×10^{-2} torr; White 1986) are given in Table 2 after correcting for the contribution from the isotope, ^{13}C.

Our ion optics, including the quadrupole deflector, are sensitive to charge variation. The trajectory of the SIMION ion beam simulation (Dahl 1995) indicates that less than 50% of all the *dications* generated by electron impact of pyrene vapor can enter the reflectron region. Therefore, the actual molar ratios of cations in the reflectron region should be approximately given by Table 3.

The SPIRE spectrum in Figure 1 (trace *b*) can thus be attributed primarily to the pyrene monocation ($C_{16}H_{10}^+$). The explicit vibrational transition frequencies of the dications are not currently available. The possible formation of PAH dications in the interstellar medium has been proposed, however, and discussed by Leach (1989, 1996) in connection with the UIR observed in H II regions. We consider these later on.

3.1. *Pyrene Cation* ($C_{16}H_{10}^+$)*: 5–9 μm Region*

Recognizing the dependence on the degree of internal excitation, both the band positions and relative intensities of SPIRE bands at 6.44 μm (=1553 cm^{-1}), 7.05 μm (=1418 cm^{-1}), 7.13 μm (=1403 cm^{-1}), 7.32 μm (=1366 cm^{-1}), 7.44 μm (=1343 cm^{-1}), 8.04 μm (=1243 cm^{-1}), 8.27 μm (=1209 cm^{-1}), and 8.41 μm (=1189 cm^{-1}) exhibit good agreement with the cryogenic matrix IR absorption spectrum (Hudgins & Allamandola 1995) and gas-phase IR

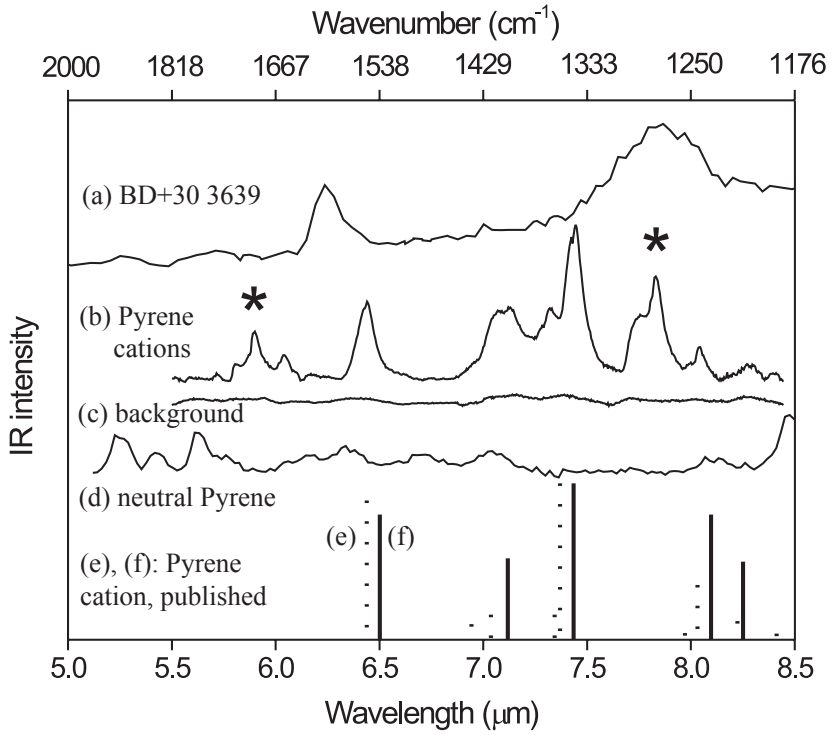

FIG. 1.—SPIRE spectrum of gas-phase pyrene cations ($C_{16}H_{10}^+$, etc.) in the 5.5–8.5 μm region when the pyrene vapor pressure was relatively low (1.0×10^{-2} torr): Trace *b* is the observed SPIRE spectrum of gas-phase pyrene cations with the background subtracted, corrected for monochromator (filters, mirrors, a diffraction grating and a detector) throughput, and its intensities are normalized. Trace *c* is the background spectrum. Trace *d* is the gas-phase SPIRE spectrum of neutral pyrene reported previously (Cook et al. 1996). The IR absorption spectra for the pyrene cation ($C_{16}H_{10}^+$) are shown in traces *e* and *f* as stick diagrams for comparison. The SPIRE spectrum in trace *b* matches well with both the matrix absorption spectrum, trace *e* (Hudgins & Allamandola 1995), and the gas-phase absorption spectrum, trace *f* (Oomens et al. 2000), except for the bands near 5.8–6.1 and 7.7–7.8 μm, marked with asterisks. The UIR spectrum from a planetary nebula, BD +30°3639, in this region is also shown in trace *a* for comparison.

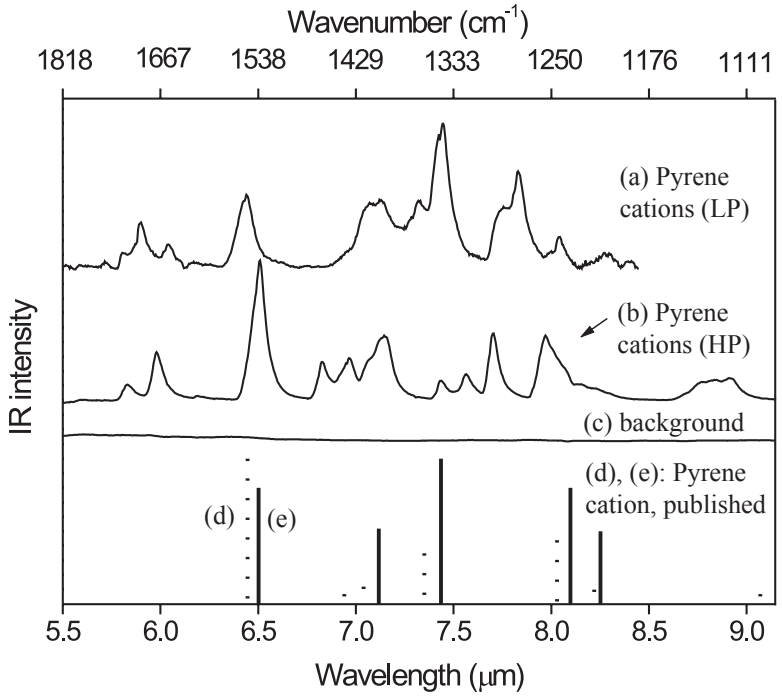

FIG. 2.—SPIRE spectra of gas-phase pyrene cations ($C_{16}H_{10}^+$, etc.) in the 5.5–9.15 μm region: Traces *a* and *b* are observed SPIRE spectra of gas-phase pyrene cations when the vapor pressure was relatively low (1.0×10^{-2} torr, LP) and high (1.5×10^{-2} torr, HP), respectively. Each spectrum is background-subtracted, and the background spectrum in trace *c* was obtained when the ions were deflected before entering the monochromator field of view under the same condition as the signal spectrum in trace *b*. The SPIRE spectrum in trace *b* was also corrected for monochromator (filters, mirrors, a diffraction grating, and a detector) throughput. The IR absorption spectra for the pyrene cation ($C_{16}H_{10}^+$) are shown in the matrix (trace *d*; Vala et al. 1994) and the gas phase (trace *e*; Oomens et al. 2000) as stick diagrams for comparison.

TABLE 1

PYRENE CATION ($C_{16}H_{10}^{+}$) FEATURES OBSERVED BY THEORY, MATRIX ISOLATION ABSORPTION, GAS-PHASE ABSORPTION, AND THE SPIRES TECHNIQUES IN THE REGION OF 2.5–9.5 μm (4000–1050 cm^{-1})

	HARMONIC, DFT[a]		GAS IR[b]		MATRIX IR[c]		MATRIX IR[d]		THIS WORK (LOW VAPOR PRESSURE, LP)[e]			THIS WORK (HIGH VAPOR PRESSURE, HP)[f]		
MODE	IF (cm^{-1})	I	IF (cm^{-1})	I	IF (cm^{-1})	I	IF (cm^{-1})	I	IF (cm^{-1})	I	FWHM (cm^{-1})	IF (cm^{-1})	I	FWHM (cm^{-1})
In-plane bend.....	1098	0.05			1102	0.07	1102	0.08		Not scanned		1124	0.17	12
							1189	0.04	1189	0.01	5			
	1214	0.09	1212	0.50	1216	0.10	1216	0.12	1209	0.08	13	1220	0.15	18
	1251	0.42	1235	0.80	1245	0.44	1245	0.34	1243	0.15	13	1245	0.37	17
							~1255	0.04						
R(C=C)	1339	0.70	1345	**1.00**	~1360	0.35	~1357	**1.00**	1343	**1.00**	18	1298	0.38	10
												1322	0.12	9
							1362	0.16	1366	0.18	12	1345	0.09	9
	1412	0.10	1405	0.52	1421	0.12	1421	0.16	1403	0.44	23	1399	0.47	16
	1433	0.16			1440	0.07	1440	0.10	1418	0.38	21	1416	0.20	19
	1533	**1.00**	1538	0.8	~1552	**1.00**	~1553	0.89	1553	0.83	25	1536	**1.00**	18
R(CH).....	3089	0.03							3077	<0.01		2990	0.01	38
									2990	<0.01				

NOTE.—IF: infrared frequencies; I: relative intensities.

[a] Langhoff 1996.

[b] Oomens et al. 2000.

[c] Vala et al. 1994.

[d] Hudgins & Allamandola 1995.

[e] See Figs. 1 (trace *b*), 2 (trace *a*), and 4 (trace *a*).

[f] See Figs. 2 (trace *b*) and 4 (trace *b*).

TABLE 2
Molar Ratio of Cations Generated by 70 V Electron Impact of Pyrene at 80°C

Cation	Ratio
$C_{16}H_{10}^{+}$	100
$C_{16}H_{9}^{+}$	11.3
$C_{16}H_{8}^{+}$	13.6
$C_{16}H_{7}^{+}$	3.2
$C_{16}H_{6}^{+}$	2.4
$C_{16}H_{10}^{2+}$	17.5
$C_{16}H_{9}^{+}$	2.6
$C_{16}H_{8}^{2+}$	12.6
$C_{16}H_{7}^{2+}$	1.9
$C_{16}H_{6}^{2+}$	2.8

absorption spectrum (Oomens et al. 2000) of the pyrene cation ($C_{16}H_{10}^{+}$), as shown in Figure 1 and Table 1. The strongest band at 7.44 μm (1343 cm^{-1}) observed in our spectrum shows a 14–17 cm^{-1} redshift relative to the bands measured in the cryogenic matrix absorption experiments and a 2 cm^{-1} redshift relative to the band measured in the gas-phase IR absorption experiments of Oomens et al. (2000).

The SPIRE spectrum covering the region of 5.5–8.5 μm, as shown in Figure 1 (trace *b*), was obtained when the oven temperature was kept relatively low (70°C, the vapor pressure of pyrene at the temperature is 1.0×10^{-2} torr; White 1986) and is reproduced in Figure 2 (trace *a*). Another SPIRE spectrum covering the region of 5.5–9.15 μm, shown in Figure 2 (trace *b*), was obtained when the vapor pressure of pyrene was 50% higher. (The oven temperature is 75°C, and the vapor pressure of pyrene at the temperature is 1.5×10^{-2} torr; White 1986.) It has been reported (Verstraete et al. 2001) that a good fit was obtained when the broad and complex 7.7 μm band of UIR observed by *Infrared Space Observatory* Short-Wavelength Spectrometer was decomposed into at least three Lorentz profiles. Accordingly, overlapped bands in the range of ~7–8.2 μm are decomposed into Lorentz profiles, and the FWHM of decomposed bands are described in Tables 1 and 4.

The major features of the observed SPIRE spectrum (except for those in the 5.8–6.1 μm [1639–1724 cm^{-1}] and 7.7–7.8 μm [1282–1299 cm^{-1}] ranges) agree well with the calculated IR spectrum, cryogenic matrix IR absorption spectra, and gas-phase IR absorption spectrum of the pyrene cation ($C_{16}H_{10}^{+}$), as shown in Figure 2 and Table 1. However, the "high-pressure" (HP) spectrum of Figure 2 (trace *b*) exhibits somewhat different spectral features from that of Figure 2 (trace *a*), despite the overall similarity of the bands to those assigned to the pyrene cation ($C_{16}H_{10}^{+}$).

TABLE 3
Actual Molar Ratio of Cations in the Reflection Region

Cation	Ratio
$C_{16}H_{10}^{+}$	100
$C_{16}H_{9}^{+}$	11
$C_{16}H_{8}^{+}$	14
$C_{16}H_{7}^{+}$	3
$C_{16}H_{6}^{+}$	2
$C_{16}H_{10}^{2+}$	<9
$C_{16}H_{9}^{2+}$	<1
$C_{16}H_{8}^{2+}$	<6
$C_{16}H_{7}^{2+}$	<1
$C_{16}H_{6}^{2+}$	<1

3.1.1. *Band Intensities*

The strongest band positions formed with the two distinct sets of experimental conditions employed in this work were different, found either at 1343 (low pressure [LP]) or at 1536 cm^{-1} (HP), as shown in Table 1. The gas-phase absorption study reported that the strongest band position is at 1345 cm^{-1}, whereas the matrix studies yield two different results. The strongest band position in the SPIRE spectrum at lower pressure is consistent with that observed in both the gas-phase experiments of Oomens et al. (2000) and the matrix study of Hudgins & Allamandola (1995). However, the strongest band position in the SPIRE spectrum at the higher pressure is consistent with that in the matrix spectrum of Vala et al. (1994). In both the experiments of Oomens et al. (2000) and Hudgins & Allamandola (1995), the vapor pressure of neutral pyrene was minimized. Oomens et al. (2000) used a shutter to reduce the deposition of neutral pyrene on the ion trap, while Hudgins & Allamandola (1995) vaporized the neutral pyrene at a relatively low temperature (60°C).

Hudgins & Allamandola (1995) and Vala et al. (1994) both used an argon matrix. However, somewhat different number densities of the neutral pyrene in the gas phase probably resulted in different number densities of the pyrene cation and the neutral pyrene (interacting with the cation) of the matrix. Hudgins & Allamandola (1995) vaporized the neutral pyrene at a relatively low temperature and ionized the neutral pyrene at 10 K *after* it had already been highly isolated in an argon matrix. However, Vala et al. (1994) ionized the neutral pyrene *before* deposition in an argon matrix at 12 K. This latter condition thus seems to produce less well-isolated pyrene cations than Hudgins & Allamandola approach, although the oven temperature was not explicitly given by Vala et al. (1994).

Since the intensity patterns of the two most nearly "collisionless" experiments (Oomens et al. 2000 and Hudgins & Allamandola 1995) are consistent with our "low-pressure" SPIRE spectrum, interactions between the neutral pyrene molecules and ions due to the higher vapor pressure (50% higher in our experiments) could be responsible for the variation in band intensities as well as band positions. Moreover, such intermolecular collisions could result in different chemistry, e.g., more probable possible formation of the pyrene dimer cation, $(C_{16}H_{10})_2^{+}$. The use of high concentrations (vapor pressure) in both the matrix and the gas-phase experiments is known to produce clusters (dimer and trimer [ion], etc.). This will be discussed later.

3.1.2. *Frequency Shifts*

The IR spectra in the experiments of Oomens et al. (2000) and Hudgins & Allamandola (1995) exhibit different band frequencies, although the two spectra show the same relative intensity pattern (see Table 1). Hudgins & Allamandola (1995) ionized the neutral pyrene by vacuum UV photolysis in an argon matrix, while Oomens et al. (2000) ionized the neutral pyrene by 193 nm excimer laser in the gas phase and confined the ions in a trap. It is well known that the shift due

TABLE 4

FEATURES OF THE DEHYDROGENATED PYRENE CATIONS ($C_{16}H_x^+$, $x = 6, 8$) OBSERVED BY THE SPIRES TECHNIQUES IN THE REGION OF 2.5–12 μm (4000–833 cm^{-1})

	HARTREE-FOCK/3-21G (PYRENE CATION AND DEHYDROGENATED PYRENE CATIONS)[a]										THIS WORK (LP)			THIS WORK (HP)			
	$C_{16}H_{10}^+$		$C_{16}H_8^+$, b		$C_{16}H_8^+$, c		$C_{16}H_6^+$, h		$C_{16}H_6^+$, e		$C_{16}H_x^+$, $x = 6, 8$			$C_{16}H_x^+$, $(C_{16}H_{10})_2^+$			
MODE	IF (cm^{-1})	GI	IF (cm^{-1})	GI	IF (cm^{-1})	GI	IF (cm^{-1})	GI	IF (cm^{-1})	GI	IF (cm^{-1})	I	FWHM (cm^{-1})	IF (cm^{-1})	I	FWHM (cm^{-1})	$(C_{16}H_{10})_2^+$
Out-of-plane bend:																	
Solo			885	42					900	41	900	0.03	6	Not scanned			
											874	0.02	5	874	0.01	2	
Duo	855	149	845–805	80	840	102	805	87	830–800	52	840	0.12	5	841	0.02	7	
In-plane bend	1200–1090	1510	1200–1050	1140	1220–1050	1198	1220–1060	2290	1250–1050	817	Not scanned			~1134	0.20	13	
R(C=C)	1490–1350	181	1490–1250	447	1470–1250	479	1470–1280	310	1450–1300	318	1277	0.39	12	1255	0.29	10	
											1291	0.22	13				
														1436	0.28	17	Probably
														1465	0.16	11	Probably
	1540	364	1590–1520	44	1560–1520	295			1520	599	The same band position as those of $C_{16}H_{10}^+$ at 1536 and 1553 cm^{-1}						
R(C≡C)			1920	101	2040	292	1920	610	1850–1720	254	1656	0.16	18				
											1695	0.36	20	1672	0.29	18	
											1721	0.05	10	1715	0.06	13	
r(CH)	3120–3030	6	3120–3030	13	3030	2	3120	4	3120	7				2990	0.01	38	Maybe
														2829	0.04	71	?
														2631	0.12	53	?

NOTE.—The calculated infrared frequencies (IF) and the integrated intensities (GI) by Pauzat et al. 1997 of $C_{16}H_{10}^+$, two isomers (b and c) of $C_{16}H_8^+$, and two isomers (h and e) among five isomers of $C_{16}H_6^+$ are reproduced in this for comparison. Tentative infrared frequencies, relative intensities (I), and the FWHM of the plausible pyrene dimer cation $(C_{16}H_{10})_2^+$ observed by the SPIRES techniques in the region of 2.5–9.5 μm (4000–1050 cm^{-1}) are also included.

[a] Pauzat et al. 1997.

to the interactions between the pyrene cation and the argon matrix produces variation in band frequencies, although different vibrational temperatures (the vibrational temperature in the cryogenic matrix experiment is probably lower) are also partially responsible. Similarly, at higher vapor pressures (either in gas-phase or matrix environments), complexation or vibrational energy transfer between the neutral pyrene molecules (cations) and the pyrene cations ($C_{16}H_{10}^+$, etc.) could be responsible for the variation in band frequencies. Space charge effects, which might vary substantially with pressure, could alter the effective residence times of the ions in our experiments and possibly those of the matrix studies as well (S. Schlemmer 2002, private communication).

Higher vapor pressure in our gas-phase experiment produced shifts in band frequencies. The strongest HP band at 1536 cm^{-1} shows a 17 cm^{-1} redshift relative to the strong LP band at 1553 cm^{-1}. Also, the aromatic CC stretching (1553–1298 cm^{-1}) and the benzyne C≡C stretching modes (see next section) observed at 5.83 μm (1715 cm^{-1}) and 5.98 μm (1672 cm^{-1}) show a redshift at HP. However, in-plane bending modes (1245–1124 cm^{-1}) exhibit a blueshift relative to those measured at LP, as shown in Tables 1 and 4.

Redshifts due to high internal energy content were also observed in our previous IR emission spectra of neutral PAHs (Cook et al. 1996, 1998). While Joblin's equation (Joblin et al. 1995), which estimates the vibrational temperature of PAHs based on the band shift, was only applied to neutral molecules, the degree of the emission band shift for a PAH cation is also likely to relate directly to the internal energy content. The higher vapor pressure conditions could facilitate collisions between the pyrene cations ($C_{16}H_{10}^+$, etc.) and the neutral pyrene molecules, leading to vibrational energy transfer (vibrational heating or cooling; Cook et al. 1998) of the pyrene cations.

Why might the SPIRE bands of the pyrene cation ($C_{16}H_{10}^+$) show noticeable frequency shifts in both the CC stretching and the CH in-plane bending mode but not in the CH out-of-plane bending, between our two distinct experimental conditions (LP and HP)? Pauzat, Talbi, & Ellinger (1997), in their theoretical calculation, showed that both the CC and CH in-plane vibrations of the pyrene cation ($C_{16}H_{10}^+$) behave similarly (and differently than the CH out-of-plane vibrations) in terms of the variation of band frequencies, relative to those of neutral pyrene. The CC and CH in-plane vibrations of the pyrene cation thus seem to have an inherent coupling; however, the CH out-of-plane vibrations seem not to be involved (dehydrogenated pyrene cations also have this coupling; Pauzat et al. 1997). Different vibrational energy distributions can result in different degrees of coupling between the vibrational modes. At HP conditions some modes, like the CC stretching, can be more vibrationally heated (producing a redshift), while other modes, like the in-plane bending, can be cooler (producing a blueshift) than with LP conditions. Thus, this vibrational coupling seems to be important to the variation in band *frequencies* of the pyrene cation between the two experimental conditions, viz., low and high vapor pressure.

Although it is not presently clear which of the two factors, "complex formation" or "collision induced vibrational redistribution/coupling," would be more important as to variation in band frequencies of the pyrene cation between the two experimental conditions (HP and LP), the two factors are probably correlated. We note that higher and lower oven temperatures will not change the rotational temperatures of the pyrene cation significantly since the difference of the oven temperatures is only 5°C. It is usually assumed that the process of electron impact does not substantially change the rotational angular momentum of a molecule; i.e., the rotational populations of the ions are the same as those of the neutral parent, given by the Boltzmann distribution (von Busch & Dunn 1972). Carrington & Tuckett (1980) showed that the increase in the rotational excitation following electron impact is minimal.

3.2. *Dehydrogenated Pyrene Cations* ($C_{16}H_9^+$, $C_{16}H_8^+$, $C_{16}H_7^+$, $C_{16}H_6^+$)

No experimental vibrational IR spectral data for the dehydrogenated pyrene cations in the 5–9.5 μm range have been reported yet, to the best of our knowledge. However, Pauzat et al. (1997) calculated the harmonic IR frequencies and integrated intensities for two isomers of the doubly dehydrogenated pyrene cation ($C_{16}H_8^+$) and for five isomers of the quadridehydrogenated pyrene cation ($C_{16}H_6^+$) at the Hartree-Fock level using Gaussian 92. Irradiation in the UV–visible range ($\lambda \geq 185$ nm) of the pyrene cations generated by electron impact showed a large increase of the $C_{16}H_8^+$ and $C_{16}H_6^+$ iso cyclotron resonance mass spectral signals, with only a small increase of the $C_{16}H_9^+$ and $C_{16}H_7^+$, at the expense of a signal intensity of pyrene molecular cation (Ekern et al. 1998). The photoproduction and apparent stability of the fragments imply that $C_{16}H_8^+$ and $C_{16}H_6^+$ may well be more important than $C_{16}H_9^+$ and $C_{16}H_7^+$ as UIR carriers in astronomical environments.

Some representative results from Pauzat et al. (1997) are reproduced in Table 4 for comparison with our experimental data. These indicate that SPIRE bands in the 5.8–6.1 μm (1639–1724 cm^{-1}) and 7.7–7.8 μm (1282–1299 cm^{-1}) ranges may well be due to dehydrogenated pyrene cations ($C_{16}H_8^+$ and $C_{16}H_6^+$). According to their calculations, as shown in Table 4, the bands due to these species show strong C≡C stretching vibrations at 4.9–5.8 μm (2040–1720 cm^{-1}) due to a benzyne triple bond, and these do not exist in the spectrum of pyrene cation. Also, the bands at 6.7–8.0 μm (1490–1250 cm^{-1}; total ranges of seven isomers) of the dehydrogenated pyrene cations are much stronger (by 1.7–2.6 times depending on isomers) and redshifted as a result of strong coupling with CH in-plane bending vibration (8–9.5 μm, 1250–1050 cm^{-1}) as compared with the bands at 6.7–7.4 μm (1490–1350 cm^{-1}), which are attributed to aromatic CC stretching vibration of the pyrene cation. Therefore, three bands at 5.81 μm (=1721 cm^{-1}), 5.90 μm (=1695 cm^{-1}), and 6.04 μm (=1656 cm^{-1}) in Figure 1 (trace *b*) can tentatively be assigned to a benzyne triple bond of the dehydrogenated pyrene cations. A strong band at 7.83 μm (=1277 cm^{-1}), with a shoulder at 7.74 μm (=1291 cm^{-1}) in Figure 1 (trace *b*) may be due to aromatic CC stretching vibrations of dehydrogenated pyrene cations that are redshifted from the strongest $C_{16}H_{10}^+$ band at 7.44 μm (1343 cm^{-1}). The observed IR bands, which tentatively ascribed to dehydrogenated pyrene cations, are summarized and compared with the theoretical results in Table 4.

The gas-phase SPIRE spectrum of the neutral pyrene reported previously is shown in Figure 1 (trace *d*). Also, the UIR spectrum from a planetary nebula, BD +30°3639 in this region is shown in Figure 1 (trace *a*) for comparison. It is striking that dehydrogenated pyrene cations show strong

emission bands at 7.7–7.8 μm, the position of the strongest band in most of the UIR. We will discuss this later on.

3.3. *The* CH *Out-of-Plane Bending Region of Pyrene Cation and Dehydrogenated Pyrene Cations*

The SPIRE spectra in Figure 3 (traces *c* an *d*) were obtained for LP and HP conditions, respectively, and with the background scan subtracted. In terms of the band positions, SPIRE bands at 11.78 μm (=849 cm^{-1}) or 11.61 μm (=861 cm^{-1}) are in reasonable agreement with the matrix data, gas-phase IR absorption data, and calculated IR bands of the pyrene cation ($C_{16}H_{10}^+$), as shown in Figure 3 (traces *e* and *f*) and in Table 5. However, relative intensities in this region are slightly lower than those reported. The relative intensities of the SPIRE bands in this region (see Table 5) are calculated relative to the strongest band at 5.5–9.15 μm. We used a 50 groove mm^{-1} grating for this region from 9.5–12 μm and a 75 groove mm^{-1} grating in the region from 5.5–9.15 μm. The relative intensities of features measured with the same grating are accurately determined, whereas the intensity comparisons of features with different gratings are somewhat less reliable, despite the correction for instrument response.

Unlike the 5.5–9.15 μm (CC stretching and CH in-plane bending) features, the SPIRE bands of the pyrene cation in the CH out-of-plane bending region did not show noticeable frequency shifts but showed the variation in band intensities between two experimental conditions, HP and LP. We discussed the possible reasons for this above.

Tentative vibrational assignments for dehydrogenated pyrene cations ($C_{16}H_8^+$ and $C_{16}H_6^+$) in this region are given in Table 4. According to calculation of Pauzat et al. (1997), dehydrogenated pyrene cations show additional bands at 885–900 cm^{-1} due to nonadjacent (solo) peripheral hydrogen atoms, and the CH out-of-plane bending mode attributed to doubly adjacent (duo) hydrogen atoms shows a redshift. Therefore, the two bands at 900 and 874 cm^{-1} may be due to dehydrogenated pyrene cations, and the band at 840–841 cm^{-1} may be due to CH out-of-plane bending vibrations of dehydrogenated pyrene cations that are redshifted from the strong band (at 849 or at 861 cm^{-1}) of the pyrene cation ($C_{16}H_{10}^+$).

3.4. *Pyrene Dimer Cation* $(C_{16}H_{10})_2^+$ *and the* CH *Stretching Region of Pyrene Cation*

Additional bands appear at 1436 and 1465 cm^{-1} in the aromatic CC stretching region under HP conditions (see Fig. 2 and Table 4), and their analogues were not observed with LP. Although the band at 1436 cm^{-1} could be assigned to the CC stretching vibration of the pyrene cation ($C_{16}H_{10}^+$), the trend of the band shift compared to the matrix data in the CC stretch region minimizes this possibility (see Tables 1 and 4). Since the two bands were observed only at the relatively high vapor pressure (i.e., higher number densities of pyrene), they may relate to a pyrene cluster

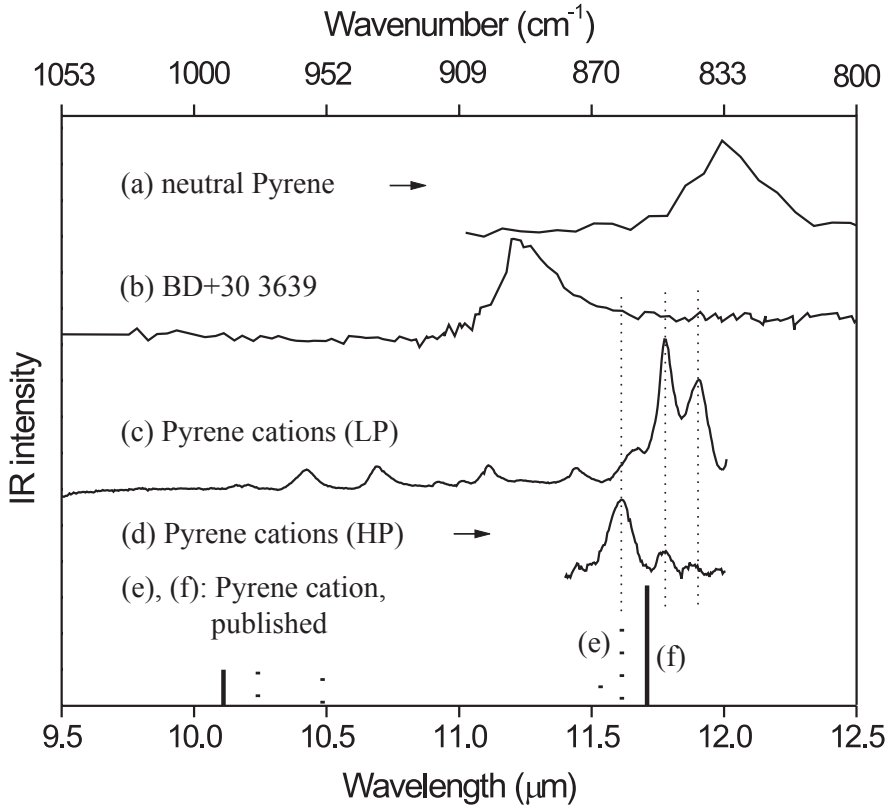

FIG. 3.—SPIRE spectra of gas-phase pyrene cations ($C_{16}H_{10}^+$ and etc.) in the 9.5–12 μm region: Traces *c* and *d* were obtained when the pyrene vapor pressure was relatively low (LP) and high (HP), respectively. Each spectrum is background-subtracted, and each background spectrum (not shown) is flat over the spectral range studied. The IR absorption spectra for the pyrene cation ($C_{16}H_{10}^+$) are shown in traces *e* and *f* as stick diagrams for comparison. Major features in the SPIRE spectra match fairly well with both the matrix absorption spectrum (trace *e*; Hudgins & Allamandola 1995) and the gas-phase absorption spectrum (trace *f*; Oomens et al. 2000). Trace *a* is the gas-phase SPIRE spectrum of neutral pyrene reported previously (Cook et al. 1996). The UIR spectrum from a planetary nebula, BD +30°3639, in this region is also shown in trace *b* for comparison.

TABLE 5

PYRENE CATION ($C_{16}H_{10}^+$) FEATURES OBSERVED BY THEORY, MATRIX ISOLATION ABSORPTION, GAS-PHASE ABSORPTION, AND THE SPIRES TECHNIQUES IN THE REGION OF 9.5–12 μm (1053–833 cm^{-1})

									THIS WORK (SPIRES)					
	HARMONIC, DFT[a]		GAS IR[b]		MATRIX IR[c]		MATRIX IR[d]		Low Vapor Pressure (LP)[e]			High Vapor Pressure (HP)[f]		
MODE	IF (cm^{-1})	I	IF (cm^{-1})	I	IF (cm^{-1})	I	IF (cm^{-1})	I	IF (cm^{-1})	I	FWHM (cm^{-1})	IF (cm^{-1})	I	FWHM (cm^{-1})
τ(CCC)	685	0.24	682	0.12	690	0.19	690	0.23			Not scanned			
Out-of-plane bend	863	0.58	854	0.45	861	0.39	861	0.27	849	0.16	5	849	0.02	3
									858	0.03	5	861	0.15	7
							867	0.04						
							954	0.07	935	0.03	6			
R(C=C)	966	0.06			976	0.05	977	0.09	959	0.03	7		Not scanned	
β(CH) ?	985	0.10	989	0.10					982	0.01	8			

NOTE.—Infrared frequencies (IF), relative intensities (I), and the FWHM of the bands are described. Tentative vibrational assignments for dehydrogenated pyrene cations ($C_{16}H_{10}^+$, $x = 6, 8$) in this region are shown in Table 4.

[a] Langhoff 1996.

[b] Oomens et al. 2000.

[c] Vala et al. 1994.

[d] Hudgins & Allamandola 1995

[e] See trace *c* in Fig. 3.

[f] See trace *d* Fig. 3.

cation, like the dimer, $(C_{16}H_{10})_2^+$. The neutral pyrene dimer has been detected in a supersonic jet (Borisevich et al. 1995); moreover, the pyrene dimer cation has been detected in glasses (Badger & Brocklehurst 1968, 1969) at 77 K, in solution (Howarth & Fraenkel 1970; Kira, Arai, & Imamura 1971), and in the gas phase (Meot-Ner 1980).

Jones, Bhattacharya, & Tiernan (1975) reported that the formation of the benzene dimer cation, generated by electron impact, depends sensitively on both the gas pressure and the electron energy, with 80 eV electron energy reported to be high enough to produce it. The benzene trimer cation was also detected in the gas phase by photoionization (Sieck & Gorden 1976) and by electron impact (Inokuchi, Ohashi, & Nishi 1997) with an electron energy of 50 eV. Therefore, our experimental conditions, viz., 70–80 eV, may well produce cluster ions, like pyrene dimer and trimer cations. Stone & Lin (1980) investigated relative yields of both benzene monomer and dimer cations as a function of the benzene pressure and observed an abrupt (twofold) increase in the yield of the benzene dimer cation at the expense of benzene monomer cation when the benzene pressure was increased by 50%—from 10 to 15 m torr. The gas pressure in our HP conditions (15 m torr) was also on the same order of magnitude as that needed to produce the benzene trimer cation (Sieck & Gorden 1976). Since our ion optics, including the quadrupole deflector, are not very sensitive to mass variation, the pyrene dimer and trimer cations, as well as the pyrene monocation itself, can indeed enter the cryogenic reflectron region, according to the trajectory of SIMION ion beam simulation (Dahl 1995). The pyrene dimer cations are known to be thermodynamically stable at low temperature (Meot-Ner 1980). Therefore, the pyrene dimer and trimer cations could indeed contribute to the SPIRE spectrum when the pyrene vapor pressure was relatively high (HP conditions, 15 mtorr).

It has been reported that an electron-impact ionization study of benzene dimer (Bz_2) yielded Bz_2^+ with 7% probability (Janda et al. 1975). In another molecular beam study (Johnson et al. 1986), the intensity ratios of benzene monomer and clusters generated by electron-impact ionization were found to be $Bz^+ : Bz_2^+ : Bz_3^+ : Bz_4^+ = 100 : 1.2 : 0.06 : 0.015$ by mass analysis. Similarly, larger PAH (like coronene and perylene) dimer cations were detected at $\sim$1% of the monomer cation intensities at low temperature (Meot-Ner 1980). Although it is not presently clear how many pyrene dimer and/or trimer cations were present under our experimental conditions, the distribution is likely to be similar to the benzene case. The yield of the pyrene dimer cation in our HP condition (15 m torr) is likely $\geq$1%, considering the sharp increase in the yield of the dimer cation with increasing gas pressure (from 10 to 15 mtorr) in the benzene case.

There are no experimental vibrational IR spectral data for pyrene dimer or trimer cations in the 5–12 μm (2000–833 cm^{-1}) range, to the best of our knowledge. However, in the CH stretching region at $\sim$3 μm, recently, Inokuchi & Nishi (2001) assigned a sharp band at 3066 cm^{-1} (3.26 μm) to a CH stretching vibration of $(C_6H_6)_2^+$ by IR photodissociation spectroscopy. They also observed two bands at 2880 cm^{-1} (3.47 μm) and 2670 cm^{-1} (3.75 μm) in the IR spectrum of $(C_6H_6)_2^+$ and attributed them to vibrational hot bands. Since the electronic structures of the rings constituting the pyrene radical cation are similar to those of the benzene radical cation, the relation between the vibrational motion and the direction of the dipole derivative of the pyrene radical cation was directly compared to those of the benzene radical cation (Torii et al. 1999). Furthermore, the CH stretching frequencies of several PAHs cations are relatively invariant to the ring size of the PAHs (Langhoff 1996; Pauzat et al. 1997). Therefore, it is likely that the CH stretching frequencies of the pyrene monomer and dimer cations are similar to those of benzene analogues.

Figure 4 shows the SPIRE spectra of gas-phase pyrene cations in the CH stretching region. Contrary to the dominance of the spectral features from pyrene cations in the 5.5–9.5 μm region (see Figs. 1 and 2), the aromatic CH stretching at $\sim$3.2–3.3 μm (3125–3030 cm^{-1}) has nearly disappeared, consistent with the theoretical predictions, as shown in Tables 1 and 4.

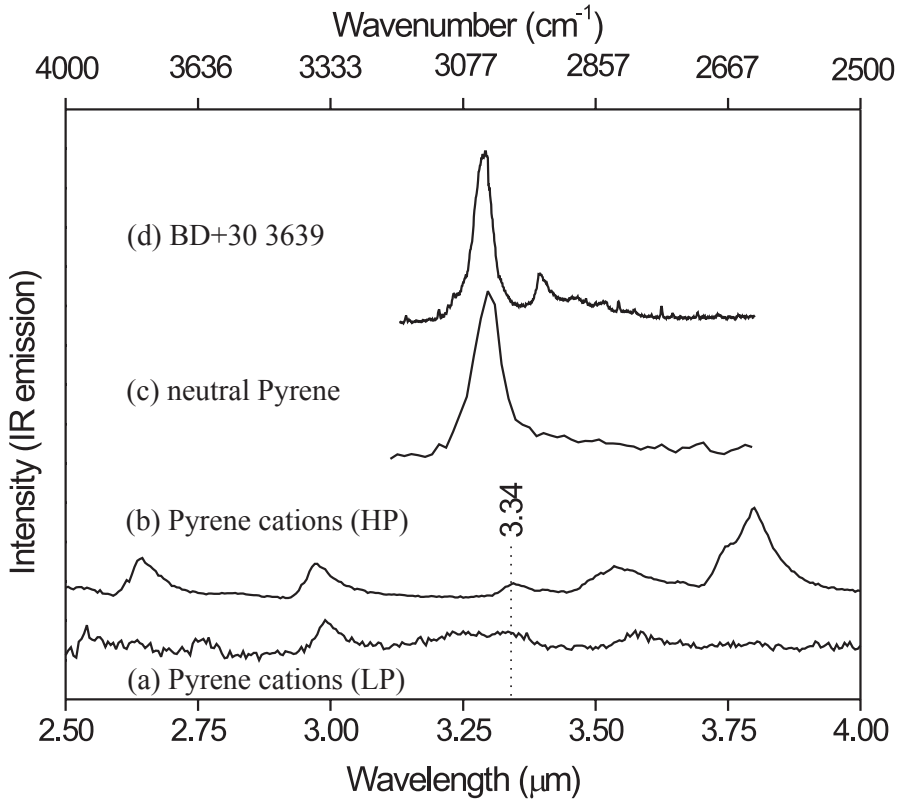

FIG. 4.—SPIRE spectra of gas-phase pyrene cations ($C_{16}H_{10}^+$ and etc.) in the 2.5–4.0 μm region: Traces *a* and *b* were obtained when the vapor pressure was relatively low (LP) and high (HP), respectively. Each spectrum is background-subtracted, and each background spectrum (not shown) is flat over the spectral range studied. Trace *c* is the gas-phase SPIRE spectrum of the neutral pyrene reported previously (Cook et al. 1996). The UIR spectrum from a planetary nebula, BD +30°3639, in this region is also shown in trace *d* for comparison.

When the pyrene vapor pressure was relatively high, the SPIRE spectrum of pyrene cations showed several weak bands at 2.64 μm (3781 cm^{-1}), 2.97 μm (3367 cm^{-1}), 3.34 μm (2990 cm^{-1}), 3.54 μm (2829 cm^{-1}), 3.75 μm (2667 cm^{-1}), and 3.80 μm (2631 cm^{-1}). When the pyrene vapor pressure was relatively low, the SPIRE spectrum of pyrene cations showed weak bands at 2.99 μm (3344 cm^{-1}), ~3.25 μm (3077 cm^{-1}), ~3.34 μm (2990 cm^{-1}), and 3.58 μm (2797 cm^{-1}). A band at 2.97 μm seems to correlate with a band at 2.99 μm, but the vibrational assignment of the band is not possible.

The bands at 3.34 μm (2990 cm^{-1}), 3.54 μm (2829 cm^{-1}), and 3.75 μm (2667 cm^{-1}) or 3.80 μm (2631 cm^{-1}) may be analogues to the bands at 3066, 2880, and 2670 cm^{-1}, respectively, which Inokuchi & Nishi (2001) attributed to the benzene dimer cation, $(C_6H_6)_2^+$. Therefore, a band at 3.34 μm (2990 cm^{-1}) may be due to a pyrene dimer cation, $(C_{16}H_{10})_2^+$, as shown in Table 4, or the band at 3.34 μm (2990 cm^{-1}) may be due to a pyrene trimer cation, $(C_{16}H_{10})_3^+$, since its position is much closer to that at 2986 cm^{-1} (3.35 μm), which was assigned (Inokuchi et al. 1997) to a C—H stretching vibration of the dimer ion core in the gas-phase benzene trimer ion, $(C_6H_6)_3^+$. Alternatively, the band at 3.34 μm (2990 cm^{-1}) may be due to the pyrene cation, $(C_{16}H_{10})^+$, since its band position is relatively close to that of the theoretical prediction (3089 cm^{-1}) and since the SPIRE spectrum (see trace *a* in Fig. 4), even under LP conditions, shows a weak spectral feature at this position.

The vibrational assignments of the CH stretching bands attributed to the pyrene cation, $(C_{16}H_{10})^+$, in this region are unclear. No experimental (matrix or gas-phase) data for pyrene cations (including dehydrogenated and dimer cations) have been reported in the 2.5–4.0 μm (4000–2500 cm^{-1}) region, probably due to the very weak spectral intensity (see Tables 1 and 4). The weak band either at ~3.25 μm (3077 cm^{-1}) or at 3.34 μm (2990 cm^{-1}) may be attributed to the pyrene cation, $(C_{16}H_{10})^+$, based on the theoretical predictions of the bands at 3.24 μm (3089 cm^{-1}) and at 3.2–3.3 μm (3120–3030 cm^{-1}), as shown in Tables 1 and 4, respectively. The other bands are not currently identified.

4. ASTROPHYSICAL IMPLICATIONS

The SPIRES features reliably assigned to the pyrene cation ($C_{16}H_{10}^+$) are described in Table 1 and are compared with the representative UIR spectrum from BD +30°3639 in the entire spectral region 3.1–12.5 μm in Figure 5. We have reduced the relative intensity of the bands at 1553 and 1536 cm^{-1} by 23% since we assigned these features to both the pyrene cation and the dehydrogenated pyrene cations (see Table 4). The value of the scaling factor of 23% is based on the molar ratios of the cations, $C_{16}H_{10}^+ : C_{16}H_9^+ : C_{16}H_8^+ : C_{16}H_7^+ : C_{16}H_6^+ = 100 : 11 : 14 : 3 : 2$.

A good agreement of the intensity distribution and a general agreement of the positions of the pyrene cation SPIRE spectrum with the UIR features is clearly seen, except for a band at 3.28 μm, thus supporting the view that cationic PAHs are good candidates for the UIR. However, the spacing (trace *d* in Fig. 5) between nominal bands at 6.2 and 7.7 μm is somewhat narrower than found in the UIR spectrum.

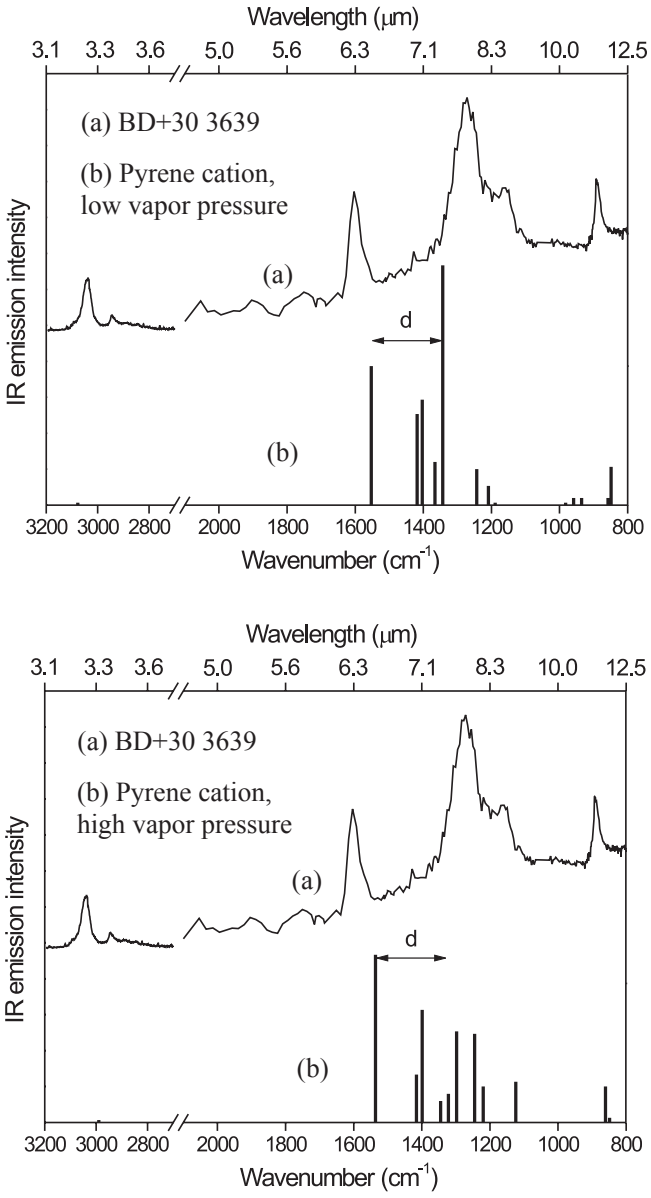

FIG. 5.—Pyrene cation ($C_{16}H_{10}^+$) SPIRE spectra with the pyrene vapor pressure relatively low (*top*) and high (*bottom*), shown here as stick spectra, compared with the UIR spectrum from BD +30°3639. The location, relative intensities, and the FWHM of each band are given in Tables 1 and 5.

Hudgins & Allamandola (1999) reported that PAH cations in the 50–80 carbon atom–size range yield spectra that are consistent with the spacing found between 6.2 and 7.6 μm (1610 and 1320 cm^{-1}) UIR bands, while those in the 20 carbon atom size provide measurable contributions to UIR based on their experimental (matrix isolation technique) spectral database of 19 cationic PAHs generated at NASA Ames. It is now quite widely believed that larger PAHs are the most probable candidates for the carriers of the UIR. Recently, Oomens et al. (2000, 2001) reported that a larger PAH-like coronene cation ($C_{24}H_{12}^+$) shows a strong infrared absorption band in the gas phase at 7.54 μm (1327 cm^{-1}), much closer to the 7.7 μm (1299 cm^{-1}) of UIR than the 7.43 μm (1345 cm^{-1}) of the pyrene cation ($C_{16}H_{10}^+$). Hence, the matrix results of Hudgins & Allamandola (1999) appear consistent with the gas-phase experiments. However, a nominal band at 6.2 μm (1610 cm^{-1}) of the gas-phase absorption spectra does not seem to follow these conclusions. The gas-phase pyrene cation shows a strong infrared absorption band at 6.50 μm (1538 cm^{-1}), closer to the 6.2 μm (1610 cm^{-1}) band of UIRs than the 6.52 μm (1533 cm^{-1}) band of coronene cation. The gas-phase IR absorption or emission spectrum of a larger PAH, like dicoronylene cation ($C_{48}H_{20}^+$), would obviously give useful information on the band at 6.2 μm.

The detailed study of dehydrogenated cations, as well as molecular ions of larger PAHs, seems necessary to further support the PAH hypothesis. Our SPIRE spectra very likely include features from dehydrogenated pyrene cations as

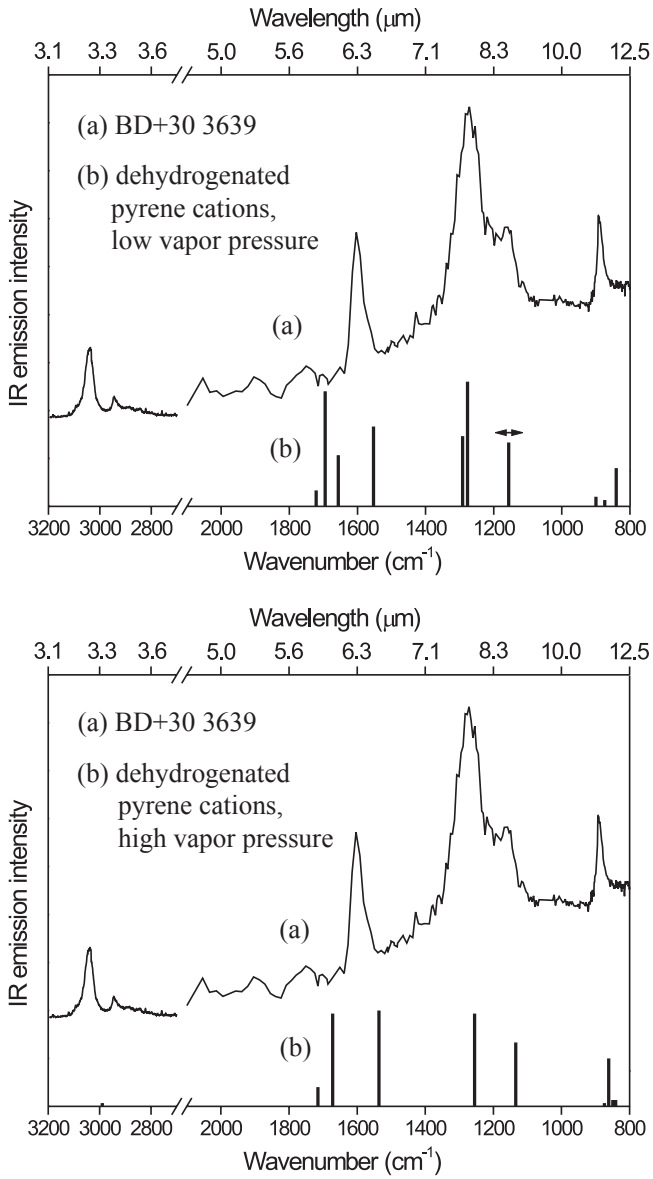

FIG. 6.—SPIRE spectra tentatively ascribed to dehydrogenated pyrene cations ($C_{16}H_x^+$, $x = 8, 6$) for the pyrene vapor pressure relatively low (*top*) and high (*bottom*), compared with the UIR spectrum from BD +30°3639. In the stick diagrams of SPIRE spectra, the location, relative intensities, and the FWHM of each band are given in Table 4. The spectral range at 1176–1050 cm^{-1} was not measured at the low vapor pressure. One band at 1156 cm^{-1} in the "top" is arbitrarily added to the stick diagram (the arrow indicates the possible variation of the band position) assuming that it will be observed, based on the trend of the band shift and on the band at 1134 cm^{-1} measured at the higher pyrene vapor pressure.

well the parent pyrene molecular ion ($C_{16}H_{10}^+$). Interestingly, we observed strong bands at 7.7–7.8 μm (assigned to dehydrogenated pyrene cations), which closely resemble the 7.7 μm of UIR. The SPIRES features of only the dehydrogenated pyrene cations summarized in Table 4 and the spectral data, for both LP and HP conditions, are compared with the representative UIR spectrum from BD +30°3639 in the entire region of 3.1–12.5 μm, as shown in Figure 6. A good general agreement of both the intensities and the positions of the SPIRE spectra assigned to dehydrogenated pyrene cations with the UIR features is found, except for a weak band at 3.28 μm, thus supporting the view that *dehydrogenated* cationic PAHs are also promising candidates for the UIR carriers. The spacing between nominal bands at 6.2 and 7.7 μm is also much closer to the UIR spectrum than found for the pyrene cation. Vuong & Foing (2000), using a model calculation, reported that in diffuse clouds, PAHs containing less than 40 carbon atoms are strongly dehydrogenated, while the partially dehydrogenated species dominate in intermediate-density clouds.

Hudgins, Bauschlicher, & Allamandola (2001) recently reported that closed-shell polycyclic aromatic hydrocarbon cations (protonated PAH cations and C_{odd} PAHs cations) are also promising candidates for UIR carriers, based on density functional theory (DFT) calculations. Closed-shell species are inherently more stable and less reactive than their open-shell counterparts. Interestingly, the intensity of the aromatic CH stretching modes of the cations increases with molecular size, approaching a value typical of neutral PAHs. Furthermore, the aromatic CC stretching modes that fall near 1600 cm^{-1}, close to the prominent 6.2–6.3 μm interstellar feature, are strongly enhanced in the closed shell cations compared with the neutral species. It would clearly be useful to study such closed-shell polycyclic aromatic hydrocarbon cations in the gas phase.

At the higher pressures used in our experiments, collisions (e.g., between neutral pyrene and pyrene cation) may actually produce the protonated pyrene cation ($C_{16}H_{11}^+$), which was reported to be much more stable than $C_{16}H_{10}^+$ and $C_{16}H_9^+$ with respect to collisional dissociation (Snow et al. 1998). Therefore, the high-pressure SPIRE spectrum presented here may have some contribution from the protonated pyrene cation ($C_{16}H_{11}^+$), although it is not presently possible to distinguish these from the IR bands attributed to the other species.

Additionally, spectra of matrix-isolated carbon nanoparticles were reported (Henning & Salama 1998) to show a UV bump (after correcting for the matrix shift) as narrow as the interstellar feature in the correct wavelength position (217.5 nm). Interstellar nanodiamonds were recently proposed to also be a promising candidate and can be heated to temperatures as high as 1000 K. Jones & d'Hendecourt (2000) suggested that expected IR bands of nanodiamonds resemble the UIRs.

The UIR mechanism implies that the carriers are much smaller (typically 1–2 nm in size according to Sellgren 1984) than classical interstellar grains (0.1 μm in size). PAH molecules and their ions are essentially small segments of carbon nanoparticles with peripheral hydrogens attached. Leach (1989) suggested that in interstellar dense clouds, collisions including neutral and ionic PAHs could form larger molecular clusters. Duley & Seahra (1998) investigated clusters of neutral PAH molecules as well as mixed ion-neutral PAH clusters and found that carbon nanostructures, formed from stacks of PAH molecules as well as dehydrogenated coronene-like molecules, exhibit the UV bump at 217.5 nm. According to the theoretical IR spectra (using a classical mechanical model), stacks of identical PAH molecules have the same vibrational modes as individual molecules (Seahra & Duley 2000), although an interaction between PAH molecules in such a stack results in an additional band between 80 and 400 μm.

The pyrene dimer cation probably has a parallel, sandwich structure in the gas phase (Meot-Ner 1980). The structure is an analog to the stacks of PAH molecules (ions), which Duley & Seahra (1998) and Seahra & Duley (2000) investigated; the stacks of PAH-like sandwich pyrene dimer (cation) could thus contribute to the UIR, especially in interstellar dense clouds. Further experimental and theoretical studies are clearly needed to sort out all of these interesting possibilities.

This work was funded by the National Aeronautics and Space Administration Astrophysics (grant NAG 5-9384) and Exobiology (grant NAG 5-7457) programs. H.-S. K. thanks the Korea Research Foundation for financial support. We thank Stephan Schlemmer and Ben McCall for critical reading of this manuscript.

REFERENCES

Allamandola, L. J., Hudgins, D. M., & Sandford, S. A. 1999, ApJ, 511, L115
Allamandola, L. J., Tielens, A. G. G. M., & Barker, J. R. 1985, ApJ, 290, L25
———. 1989, ApJS, 71, 733
Badger, B., & Brocklehurst, B. 1968, Nature, 219, 263
———. 1969, Trans. Faraday Soc., 65, 2588
Bernstein, M. P., Sandford, S. A., Allamandola, L. J., Gillette, J. S., Clemett, S. J., & Zare, R. N. 1999, Science, 283, 1135
Borisevich, N. A., Vodovatov, L. B., D'Yachenko, G. G., Petukhov, V. A., & Semenov, M. A. 1995, Opt. Spektrosk., 78, 241
Brion, C. E., & Hamnett, A. 1981, Adv. Chem. Phys., 45, 2
Carrington, A., & Tuckett, R. P. 1980, Chem. Phys. Lett., 74, 19
Cook, D. J., Schlemmer, S., Balucani, N., Wagner, D. R., Harrison, J. A., Steiner, B., & Saykally, R. J. 1998, J. Phys. Chem. A, 102, 1465
Cook, D. J., Schlemmer, S., Balucani, N., Wagner, D. R., Steiner, B., & Saykally, R. J. 1996, Nature, 380, 227
Dahl, D. A. 1995, SIMION 3D Version 6.0 Idaho, Nat. Eng. Lab. Rep. No. INEL-95/0403
Duley, W. W., & Seahra, S. 1998, ApJ, 507, 874
Ekern, S. P., Marshall, A. G., Szczepanski, J., & Vala, M. 1998, J. Phys. Chem. A, 102, 3498
Engelhardt, C., Keske, J. C., Rees, F. S., Self-Medlin, Y. B., Yoo, H. S., & Pate, B. H. 2001, J. Phys. Chem. A, 105, 6800
Furuya, K., Koto, E., & Ogawa, T. 1996, Chem. Phys. Lett., 253, 87
Henning, T., & Salama, F. 1998, Science, 282, 2204
Howarth, O. W., & Fraenkel, G. K. 1970, J. Chem. Phys., 52, 6258
Hudgins, D. M., & Allamandola, L. J. 1995, J. Phys. Chem., 99, 3033
———. 1999, ApJ, 513, L69
Hudgins, D. M., Bauschlicher, C. W., & Allamandola, L. J. 2001, Spectrochim. Acta, 57, 907
Inokuchi, Y., & Nishi, N. 2001, J. Chem. Phys., 114, 7059
Inokuchi, Y., Ohashi, K., & Nishi, N. 1997, Chem. Phys. Lett., 279, 73
Janda, K. C., Hemminger, J. C., Winn, J. S., Novick, S. E., Harris, S. J., & Klemperer, W. 1975, J. Chem. Phys., 63, 1419
Joblin, C., Boissel, P., Léger, A., d'Hendecourt, L., & Défourneau, D. 1995, A&A, 299, 835
Joblin, C., d'Hendecourt, L., Léger, A., & Défourneau, D. 1994, A&A, 281, 923
Johnson, R. D., Burdenski, S., Hoffbauer, M. A., Giese, C. F., & Gentry, W. R. 1986, J. Chem. Phys., 84, 2624
Jones, A. P., & d'Hendecourt, L. 2000, A&A, 355, 1191
Jones, E. G., Bhattacharya, A. K., & Tiernan, T. O. 1975, Int. J. Mass Spectrom. Ion Processes, 17, 147

Keller, J. W., Coplan, M. A., & Goruganthu, R. 1992, ApJ, 391, 872
Khakoo, M. A., Ratliff, J. M., & Trajmar, S. 1990, J. Chem. Phys., 93, 8616
Kim, H.-S., & Saykally, R. J. 2002, Rev. Sci. Instrum, in press
Kim, H.-S., Wagner, D. R., & Saykally, R. J. 2001, Phys. Rev. Lett., 86, 5691
Kira, A., Arai, S., & Imamura, M. 1971, J. Chem. Phys., 54, 4890
Kwok, S., Volk, K., & Bernath, P. 2001, ApJ, 554, L87
Langhoff, S. R. 1996, J. Phys. Chem., 100, 2819
Leach, S. 1989, in IAU Symp. 135, Interstellar Dust, ed. L. J. Allamandola & A. G. G. M. Tielens (Dordrecht: Kluwer), 155
———. 1996, Z. Phys. Chem., 195, 15
Léger, A., & d'Hendecourt, L. 1989, Ann. Phys., 14, 181
Léger, A., & Puget, J. L. 1984, A&A, 137, L5
Maier, J. P., & Marthaler, O. 1978, Chem. Phys., 32, 419
Meot-Ner, M. 1980, J. Phys. Chem., 84, 2724
Oomens, J., van Roij, A. J. A., Meijer, G., & von Helden, G. 2000, ApJ, 542, 404
Oomens, J., Sartakov, B. G., Tielens, A. G. G. M., Meijer, G., & von Helden, G. 2001, ApJ, 560, L99
Pauzat, F., Talbi, D., & Ellinger, Y. 1997, A&A, 319, 318
Petroff, M. D., Stapelbroek, M. G., & Kleinhans, W. A. 1987, Appl. Phys. Lett., 51, 406
Rouan, D., Léger, A., Omont, A., & Giard, M. 1992, A&A, 253, 498
Schlemmer, S., Cook, D. J., Harrison, J. A., Wurfel, B., Chapman, W., & Saykally, R. J. 1994, Science, 265, 1686
Seahra, S. S., & Duley, W. W. 2000, ApJ, 542, 898
Sellgren, K. 1984, ApJ, 277, 623
Sieck, L. W., & Gorden, R., Jr. 1976, Int. J. Mass Spectrom. Ion Phys., 19, 269
Snow, T. P., Le Page, V., Keheyan, Y., & Bierbaum, V. M. 1998, Nature, 391, 259
Stone, J. A., & Lin, M. S. 1980, Can. J. Chem., 58, 1666
Tielens, A. G. G. M. 1997, Ap&SS, 251, 1
Torii, H., Ueno, Y., Sakamoto, A., & Tasumi, M. 1999, J. Phys. Chem. A, 103, 5557
Vala, M., Szczepanski, J., Pauzat, F., Parisel, O., Talbi, D., & Ellinger, Y. 1994, J. Phys. Chem., 98, 9187
Verstraete, L., et al. 2001, A&A, 372, 981
von Busch, F., & Dunn, G. H. 1972, Phys. Rev. A, 5, 1726
Vuong, M. H., & Foing, B. H. 2000, A&A, 363, L5
Wacks, M. E. 1964, J. Chem. Phys., 41, 1661
Wagner, D. R. 2001, Ph.D. thesis, Univ. California, Berkeley
Wagner, D. R., Kim, H.-S., & Saykally, R. J. 2000, ApJ, 545, 854
White, C. M. 1986, J. Chem. Eng. Data, 31, 198
Wong, S. F., & Schulz, G. J. 1975, Phys. Rev. Lett., 35, 1429